CHAPTER 6

THE PROXIMITY FED RECTANGULAR PATCH MICROSTRIP ANTENNA

6.1 Introduction

As discussed in Chapter 5, the Microstrip Antenna (MSA) is a low profile, conformable, light weight, easily manufactured antenna. The MSA is a resonant structure consisting of a dielectric substrate sandwiched between a metallic patch and a ground plane. The metallic patch is often excited using either a coaxial probe feed or a microstrip edge feed. The outer conductor of the coaxial probe feed is connected to the ground plane. The center conductor protrudes through the ground plane and dielectric substrate to contact and excite the patch. The microstrip edge feed is a microstrip feedline that contacts the edge of the patch. The coaxial probe feed and microstrip edge feed are contacting feeds. That is, they excite the patch by directly contacting it. The greatest disadvantage of the MSA fed using a contacting feed is inherently low impedance bandwidth. One way to increase the bandwidth of the MSA is to use a non-contacting feed. The aperture coupled MSA and the proximity-fed MSA, presented in Section 5.3.4, are non-contacting feeds. In this chapter, a proximity coupled rectangular microstrip patch antenna is modeled numerically using the Method of Moments (MoM). In Section 6.2, a numerical MoM algorithm that is applicable to planar circuits and antennas is presented and verified. In Section 6.3, the MoM is used to study the proximity coupled patch antenna developed by Pozar in [1]. The input impedance and radiation patterns of a proximity coupled rectangular patch antenna are modeled in Section 6.3.1. The effects of changes in patch and feed geometry on input impedance are described in Section 6.3.2.

Finally, a single open-circuit shunt stub is used to tune the antenna to an arbitrary feedline in Section 6.3.3. Concluding remarks are found in Section 6.4.

6.2 Method of Analysis

6.2.1 Application of the Method of Moments to Planar Antennas using SONNET

The analysis in this chapter uses a commercially available software package called SONNET to apply the Method of Moments (MoM) to the proximity coupled microstrip patch antenna. The algorithm used by SONNET is designed to model planar circuits within a rectangular conducting grounded shield. The process used by SONNET to model planar circuits is summarized in four steps: [2]

1. The metallization is subdivided into small rectangular overlapping subsections.
2. An explicit current distribution is assumed on each subsection.
3. The current magnitude in each subsection is adjusted such that the tangential electric field goes to zero at the surface of every conductor.
4. The circuit parameters are derived using the current magnitudes determined in step 3.

Consider a microstrip circuit that is completely contained within a conducting box as shown in Figure 6.1. The metallization is printed on a substrate with dielectric constant ε_1 and thickness *h*. Another dielectric layer is located above the metallization. In this case the upper layer is air.

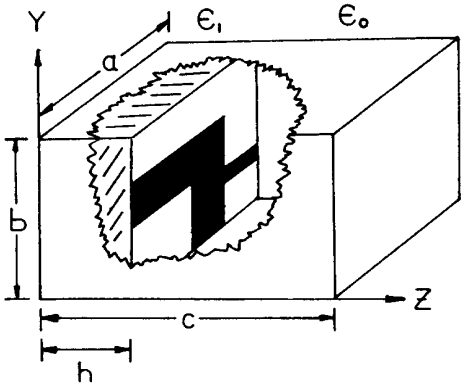

Figure 6.1. A microstrip circuit contained within a rectangular conducting box. [2]

The conducting box is treated as two separate waveguides connected at $z=h$. [2] The fields in both waveguides are written as a sum of homogenous waveguide modes that depend on dielectric constant, ε_r, and permeability, μ, of the filler material, radian frequency, ω, and height of the waveguide, h. [2] The height of the waveguide corresponds to the thickness of the dielectric layer. The modes are expanded along a set of orthonormal mode vectors that are determined by the shape of the conducting shield. [2]

Since the environment is not free space, a Green's function is derived in the spatial domain for the currents on the surface of the substrate. [2] The surface current on the circuit is determined by subdividing the metallization into a number of small rectangular subsections. A rooftop distribution is used to expand the current onto each subsection. [2] The rooftop distribution in Figure 6.2 is separable in the x and y dimensions. It is a triangle function in the direction of current flow, and a rectangle function in the lateral direction. [2]

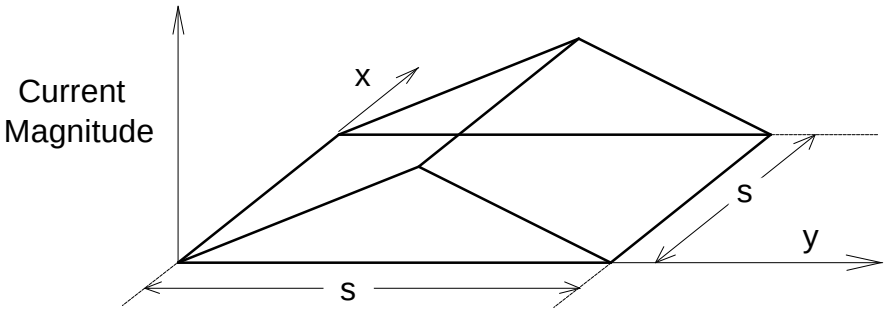

Figure 6.2. The rooftop current distribution.

Once the current is expanded into all of the subsections using the distribution in Figure 6.2, the MoM is used to adjust the magnitude and phase of the current on each subsection such that the tangential electric field at all conducting surfaces is zero. [2] The MoM algorithm developed in Chapter 4 used a delta weighting function at the center of each segment. This is called a point matching technique, and corresponds to sampling the wave function at the center of each segment. The SONNET algorithm uses a weighting function that is identical to the current expansion function so that the currents and fields are weighted identically. This is called a Galerkin's method. [2] Implementing the MoM solution, the desired circuit parameters follow directly from the modeled surface currents.

6.2.2 Feed and Field Modeling in SONNET

The feed configuration used by SONNET is applicable to any of the feeds described in Section 6.1. SONNET models fields as a sum of homogenous waveguide modes that exist within a rectangular conducting box. Therefore, antennas modeled using SONNET are operated within a rectangular conducting box of finite dimensions. The feed is coaxial. The shield of the coaxial line is attached to the conducting box, and the center conductor excites an adjacent subsection called the port subsection. The current on the port subsection is distributed using the rooftop distribution. The tangential electric field on the port subsection is set to a constant value. On all other subsections, the tangential electric field is forced to zero. This is similar to the gap source model used by NEC4 (see Section 4.2.2.2). The input admittance at the port subsection is [2]

$$Y_p = -\frac{I_p^2}{\iint \mathbf{E} \cdot \mathbf{J}\, ds} \tag{6.1}$$

where I_p is the input current at the port subsection, **E** is the tangential electric field, and **J** is the current density. By definition, **E** is zero everywhere except at the port subsection, so only this subsection is considered. [2] The weighted integral of the electric field on the port subsection is one. The current on the port subsection is proportional to the electric field weighting function since a Galerkin Method was used. The constant of

proportionality is Y_{11}. Thus, the integral in the denominator of (6.1) is identical to Y_{11}. [2] The input current at the port subsection is the input current density, $J_1 = Y_{11}$, multiplied by the width of the input subsection in the direction of current flow, Δw. [2] Thus, [2]

$$Y_p = \frac{-\left(Y_{11}\Delta w\right)^2}{Y_{11}} = -Y_{11}\left(\Delta w\right)^2 \qquad (6.2)$$

gives the input admittance and, thus, the input impedance of the antenna or circuit.

The method used to calculate the far-field radiation of the antenna is not specifically defined in the SONNET documentation or references. The SONNET software package includes a routine called PATGEN that implements a solution of the far-field radiation pattern, but the algorithm is not included in the documentation. However, the documentation contains an example that compares the fields calculated for a infinitesimal current source above a ground plane calculated using PATGEN to the canonical solution found in the literature. The solutions are identical. [3]

In the next section, SONNET is used to model a conventional half-wave rectangular probe fed microstrip patch antenna in an open environment. The methods used by SONNET to calculate input impedance and far-field radiation are verified by comparing the results to those for an identical patch treated using the magnetic cavity model established in Section 5.2.1.

6.2.3 Application of SONNET to Free Space Radiation Problems

The SONNET algorithm is designed to treat planar circuits that operate inside a rectangular conducting box. Therefore, the extension to free space radiation problems is not obvious. However, the SONNET User's Manual lists five conditions under which a free space approximation is valid. The conditions are easily violated, and unless the analysis is carefully prepared, the algorithm is likely to yield incorrect results. [3] However, when all five guidelines are satisfied, useful, but approximate, results for input impedance and far-field radiation pattern are obtained. [3]

First Condition: *Both of the lateral substrate dimensions, a and b, must be greater than one or two wavelengths.*

If the walls that make up the waveguides in Figure 6.1 are too close together, the number of non-vanishing homogenous modes in the summation is limited. This is not the free space condition and impedance and pattern calculations are corrupted. [3]

Second Condition: *The sidewalls of the conducting box must be far enough from the radiating structure so that that they have no effect.*

If the walls of the waveguide are close to the radiating structure, surface currents are coupled to them. The result is an imaging effect that creates the equivalent of another radiating structure behind the sidewall. Therefore, the sidewall spacings, which are equivalent to the substrate dimensions *a* and *b*, must be as large as possible.

The validity of conditions 1 and 2 is tested by observing the impedance results for increments of sidewall spacing until convergence is obtained. That is, Z_{in} is evaluated for $a + \Delta a$ and $b + \Delta b$ until the results converge. The sidewall spacings, *a* and *b*, are then valid, assuming the impedance converges to a reasonable answer. [3]

Third Condition: *Place the top cover outside the near field of the radiating structure.*

This condition prevents the resistive top cover of the waveguide from interfering with the reactive near fields of the radiating structure. If the condition is violated, the input reactance is invalid. The top cover spacing, *c*, must be at least a half-wavelength to satisfy this condition. [3]

Fourth Condition: *Set the top cover resistivity to 377 Ohms/square.*

This matches the resistance of the top cover, Z_{tc}, to that of free space ($\eta = 377\ \Omega$). Thus, the top cover is effectively removed and resonances due to the closed box are avoided. However, $Z_{tc} = 377\ \Omega$ is a compromise because TE modes have modal impedances higher than 377 Ω, and TM modes have modal impedances lower than 377 Ω. If the waveguide is large in both lateral dimensions (condition 1), all of the modal impedances approach 377

Ω, and reflection from the top cover is minimized. The effect is further limited if the top cover is located far away from the radiating structure ($c >> \lambda$). [3]

Fifth Condition: *The surface can not generate a significant surface wave.*

This is true because surface waves will be reflected by the conducting sidewalls and will cause inaccurate results. Surface waves are generated within thick substrates. Therefore, when thick dielectric substrates are used special attention is required to verify the absence of surface wave effects in the results. [3]

In the following section, the validity of the five free space conditions is tested by modeling a rectangular microstrip patch antenna in free space using SONNET. Convergence tests are performed to determine proper subsectioning, sidewall placement, and top cover placement. The results of the SONNET model are compared to those of the magnetic cavity model that was developed in Section 5.2.1.

6.2.4. Verification of the SONNET Algorithm

6.2.4.1. Convergence Tests

In the previous section, a MoM algorithm was developed that is applicable to planar microstrip antennas (MSAs) in free space. In this section the algorithm is verified and applied to the probe fed rectangular patch antenna in Figure 6.3. The dimensions of the MSA in Figure 6.3 are in Table 6.1. Convergence tests are used to determine valid MoM subsectioning, and SONNET sidewall placement (*a* and *b*), and top cover placement (*c*).

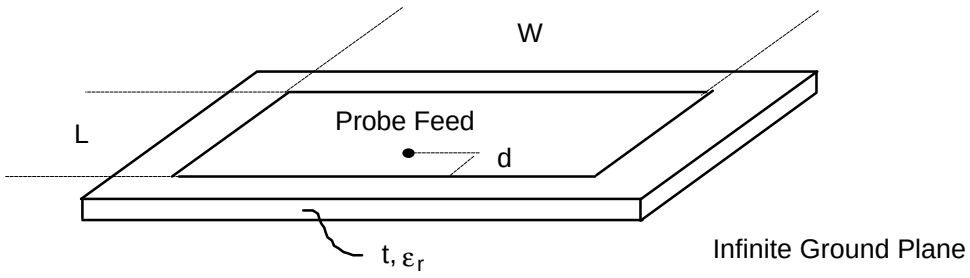

Figure 6.3. A probe fed rectangular microstrip patch antenna

Table 6.1. The dimensions of the rectangular patch MSA in Figure 6.3.

Quantity	Symbol	Value	Unit
Resonant Frequency	f_r	3.49	GHz
Patch Length	L	27.5	mm
Patch Width	W	40	mm
Substrate Material		Duroid 5880	--
Dielectric Constant	ε_r	2.20	--
Substrate Thickness	t	1.58	mm
Feed Point	d	7.5	mm

First, a convergence test was used to determine the required number of current subsections on the MSA in Figure 6.3. Figure 6.4 shows the modeled input impedance for three different current subsection representations. In Figure 6.4(a), the rectangular patch is made up of 704 square subsections with the length of each side, s = 0.125 cm. In Figure 6.4(b) there are 176 square subsections with s = 0.25 cm. Figure 6.4(c) shows the input impedance a patch consisting of 2816 square subsections with s = 0.0625 cm. Figure 6.4 shows that the modeled input impedance of the proximity coupled rectangular patch antenna changes as the number of current subsections is increased. The difference in input impedance shown in Figures 6.4(a&b) is the same as that shown in Figures 6.4(a&c).

However, the required computation time using a Pentium 100 processor is 1 minute per frequency when 176 subsections are used, 1.5 minutes per frequency when 704 subsections are used, and 15 minutes per frequency when 2816 subsections are used. Therefore, 704 subsections is a good trade-off between accuracy and required computation time. Thus, the SONNET models in this chapter use square subsections with s = 0.125 cm and a total of 704 current subsections in the MoM representation of the patch.

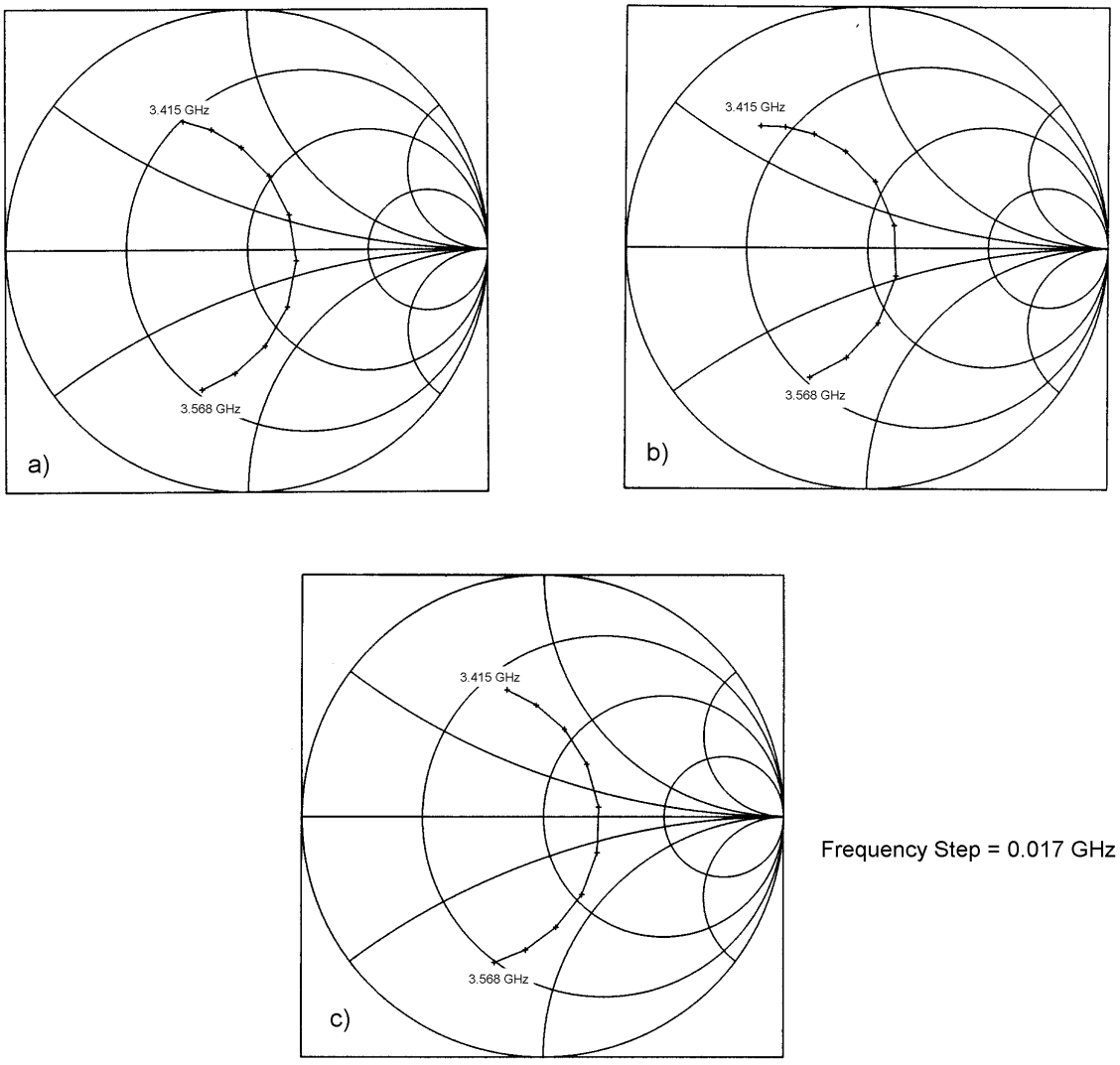

Figure 6.4. The input impedance (calculated using SONNET) of the rectangular patch antenna in Figure 6.3 using a) 704 subsections, b) 176 subsections c) 2816 subsections.

After the appropriate number of current subsections was determined, the effects of the SONNET sidewall spacings, *a* and *b*, were studied using a similar convergence test. Figure 6.5 shows the modeled input impedance for different sidewall spacings (*a* and *b* in Figure 6.1). The SONNET models in this chapter use a shielding box with $a = b$. In Figure 6.5(a), $a = b = 1.5\lambda$. In Figure 6.5(b), $a = b = \lambda$. In Figure 6.5(c), $a = b = 2.5\lambda$.

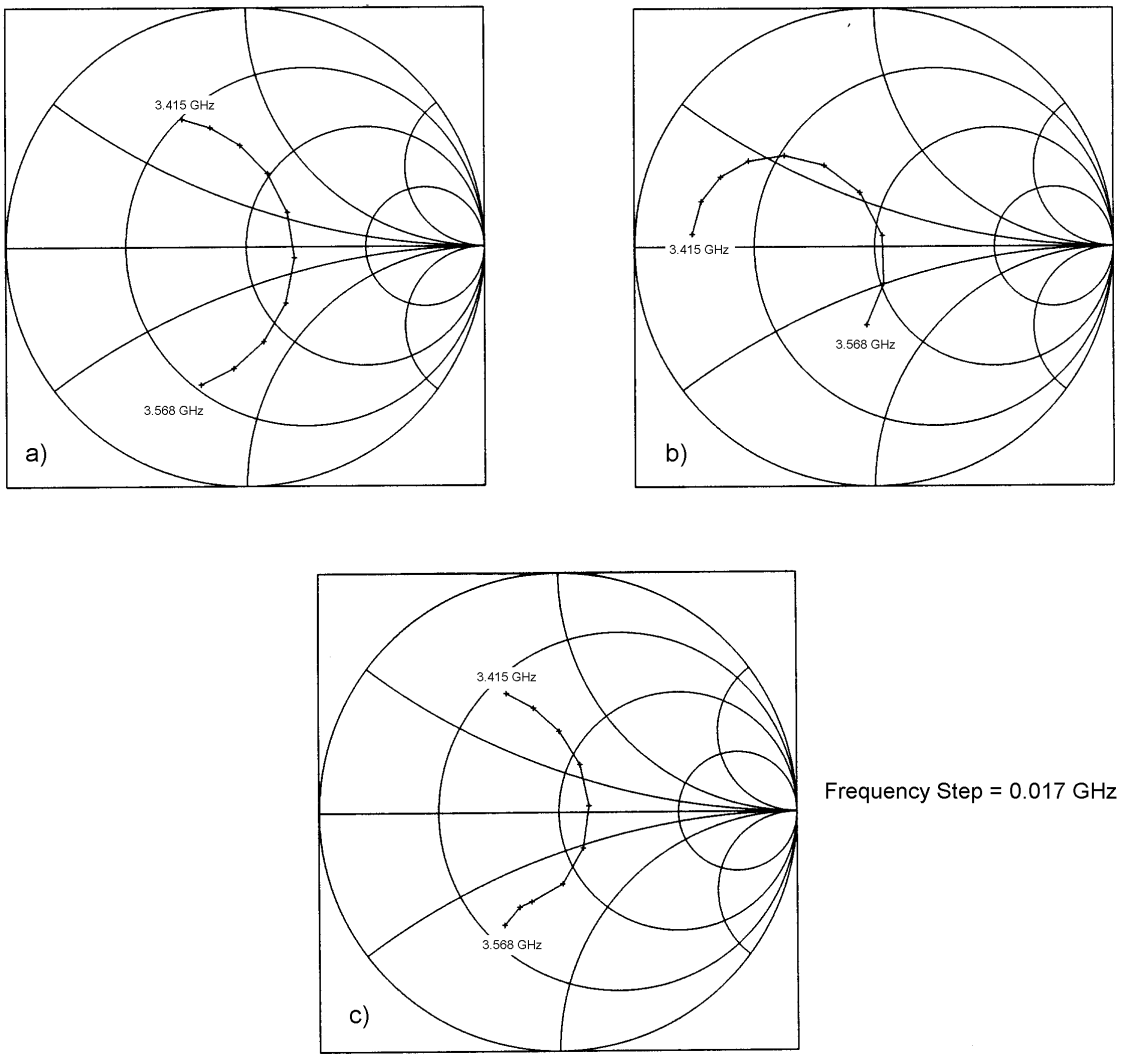

Figure 6.5. The input impedance (calculated using SONNET) of the rectangular patch antenna in Figure 6.3 using SONNET with a) $a = b = 1.5\lambda$, b) $a = b = \lambda$ c) $a = b = 2.5\lambda$.

The discrepancy between the impedances shown in Figures 6.5(a&b) is much greater than that shown in Figures 6.5(a&c). Therefore, convergence is inferred at 1.5λ since Z_{in} is the same for $a = b = 1.5\lambda$ as it is for $a = b = 2.5\lambda$. The convergence indicates satisfaction of free space conditions 1 and 2. Increasing the sidewall spacings increases the required matrix fill and reduce times since the entire region within the walls is subsectioned. The added accuracy achieved for sidewall spacings greater than $a = b = 1.5\lambda$ is not worth the added computation time. Therefore, the sidewall spacings used in the rest of the chapter are $a = b = 1.5\lambda$.

Finally, a convergence test is used to determine a valid SONNET top cover location, *c*. Figure 6.6 shows the input impedances for different locations of the conducting box top cover. Figure 6.6(a) shows the input impedance for $c = \lambda$. In Figure 6.6(b), $c = 2.5\lambda$. In Figure 6.6(c), $c = 6\lambda$. Figure 6.6 shows that the input impedance does not converge with increasing top cover location, *c*. For top cover locations greater than a wavelength, numerical instabilities occur. As the complexity of the numerical model increases, the numerical instability becomes more severe. As shown in Figures 6.6(b&c) the shape of the impedance locus changes even when the top cover is located six wavelengths away. Incremental testing shows that instability rarely occurs for top cover placements equal to a wavelength, a value that satisfies free space condition 3. Therefore, $c = \lambda$ is used in the remainder of the chapter.

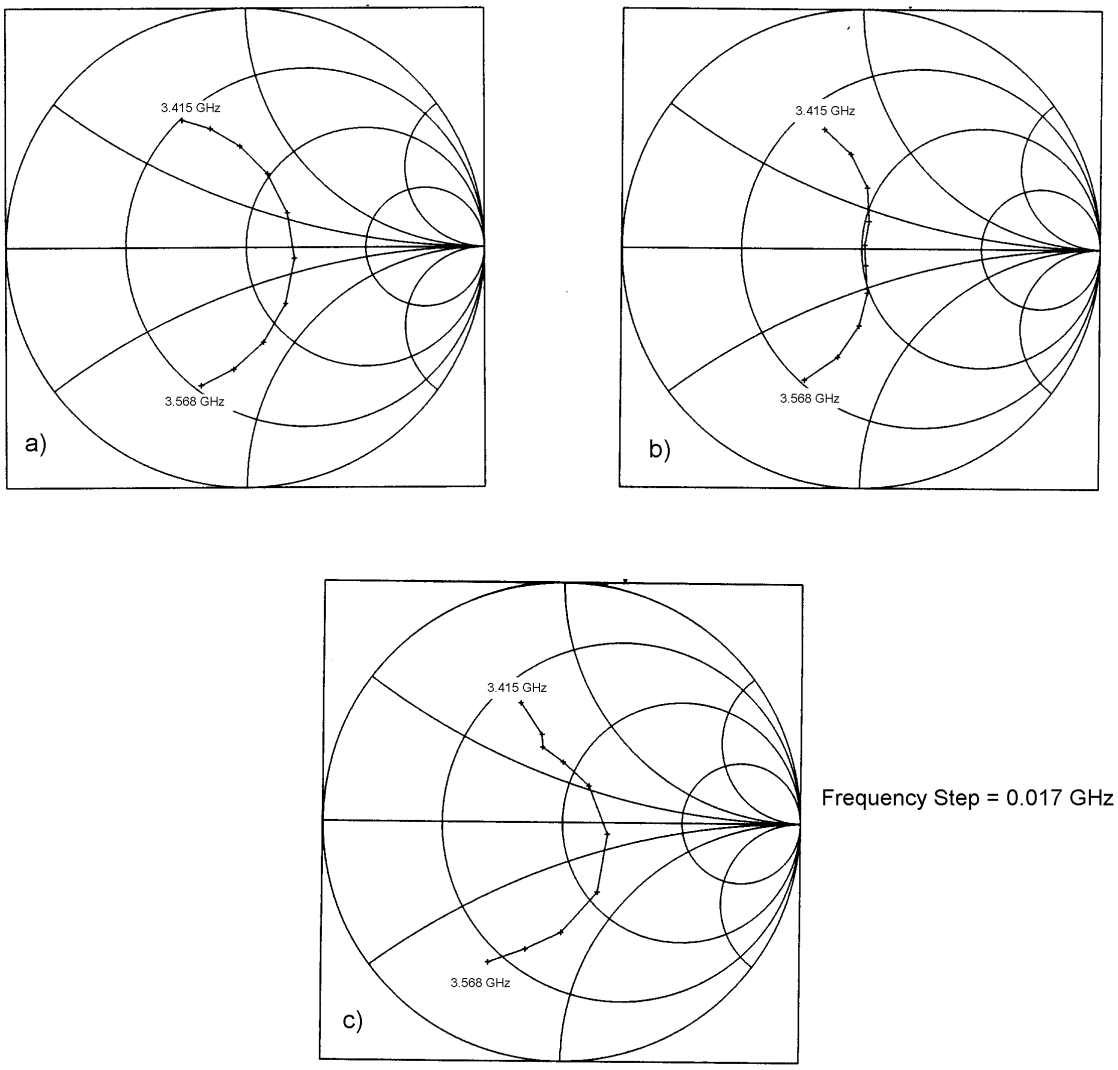

Figure 6.6. The input impedance (calculated using SONNET) of the rectangular patch antenna in Figure 6.3 using a) $c = \lambda$, b) $c = 2.5\lambda$ c) $c = 6\lambda$.

6.2.4.2 Application of SONNET to the Rectangular Patch MSA

In this section, the modeling parameters developed in Section 6.2.4.1 are verified by calculating the input impedance and far-field radiation patterns of the rectangular patch MSA in Figure 6.3 (with the dimensions specified in Table 6.1) using SONNET and comparing the results to those calculated using the magnetic cavity model developed in

Section 5.2.1. Figure 6.7 shows the input impedance of the MSA in Figure 6.3 modeled using SONNET.

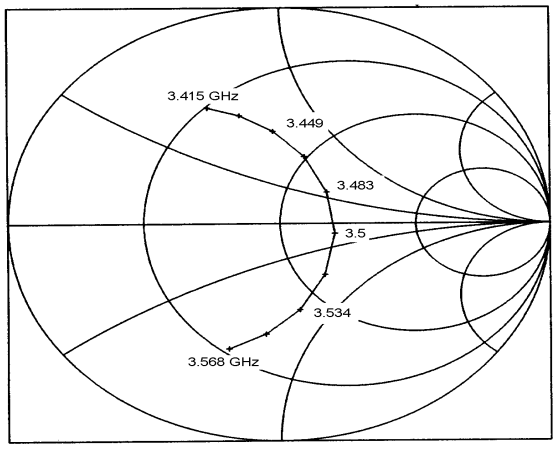

Figure 6.7. The input impedance of the rectangular patch antenna in Figure 6.3 using the dimensions in Table 6.1, modeled using SONNET and $a = b = 1.5\lambda$, $c = \lambda$, and $Z_{tc} = 377\ \Omega$.

The E-plane and H-Plane patterns of the rectangular patch antenna, modeled using SONNET and generated using PATGEN, are illustrated in Figure 6.8.

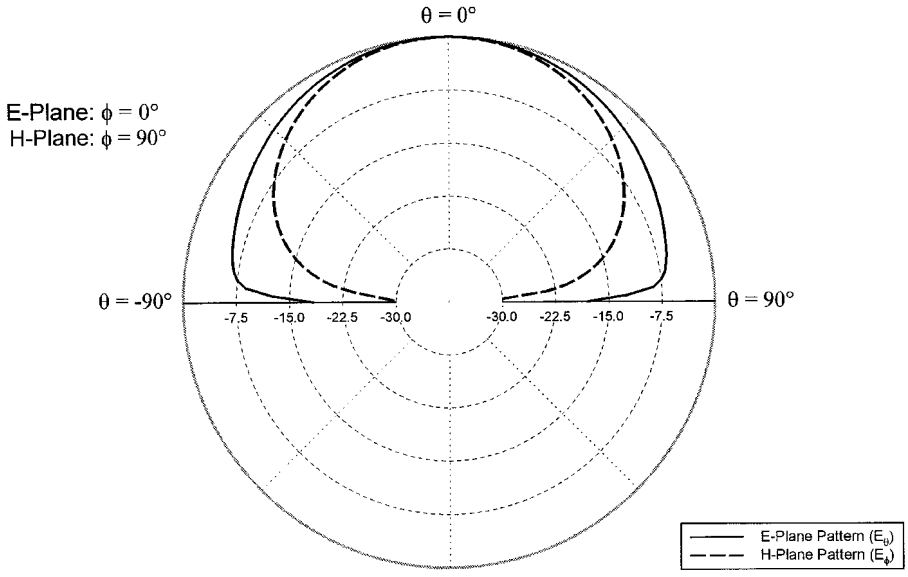

Figure 6.8. The far-field radiation patterns of the rectangular patch antenna in Figure 6.3 using the dimensions in Table 6.1, modeled using SONNET and $a = b = 1.5\lambda$, $c = \lambda$, and $Z_{tc} = 377\ \Omega$.

The E-plane pattern in Figure 6.8 has a 3 dB beamwidth of 96°. The H-plane pattern has a 3 dB beamwidth of 72°. To verify the SONNET results, a commercially available routine called PCAAD is used to calculate the input impedance of the MSA in Figure 6.3 using the magnetic cavity model. The resulting input impedance is illustrated in Figure 6.9.

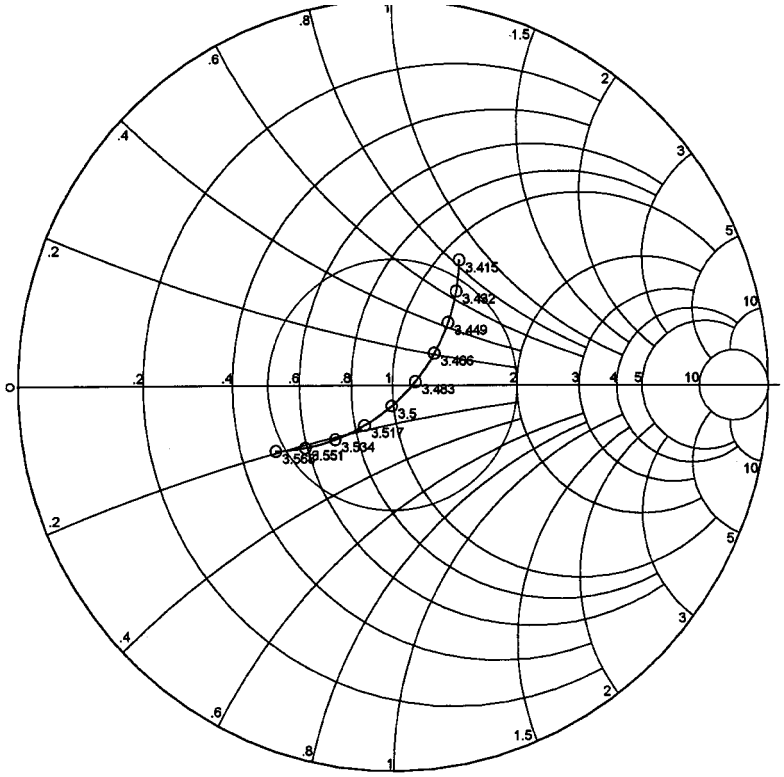

Figure 6.9. The input impedance of the rectangular patch antenna in Figure 6.3, modeled using the cavity model in Section 5.2.1.

The input impedance modeled using SONNET closely matches the cavity model result. The cavity model input impedance is rotated slightly in a clockwise direction around the center of the Smith Chart, indicating the addition of capacitance. However, the shapes of the impedance locuses are identical. The E-Plane and H-Plane radiation patterns of the rectangular patch antenna calculated using the magnetic cavity model are illustrated in Figure 6.10.

The patterns in Figure 6.10 and Figure 6.8 are nearly identical. The 3 dB beamwidth of the E-plane pattern obtained using the cavity model is 102°, 6° wider than the SONNET result. The 3 dB beamwidth of the H-plane pattern in Figure 6.10 is 72°, which is identical to the SONNET result. An unexpected null is formed in the equatorial plane ($\theta = \pm 90°$) of the SONNET E-plane pattern. Neglecting this null, the patterns show agreement between the two modeling methods. Since the impedance and patterns modeled by SONNET match those modeled using the cavity model, the validity of both methods is supported. The agreement of the results also indicates that the numerical results are converging to the correct answer and that the five free space conditions are satisfied. In the next section, the proximity-fed rectangular patch MSA is modeled using SONNET and the modeling parameters (*a*, *b*, *c*, and Z_{tc}) established in this chapter.

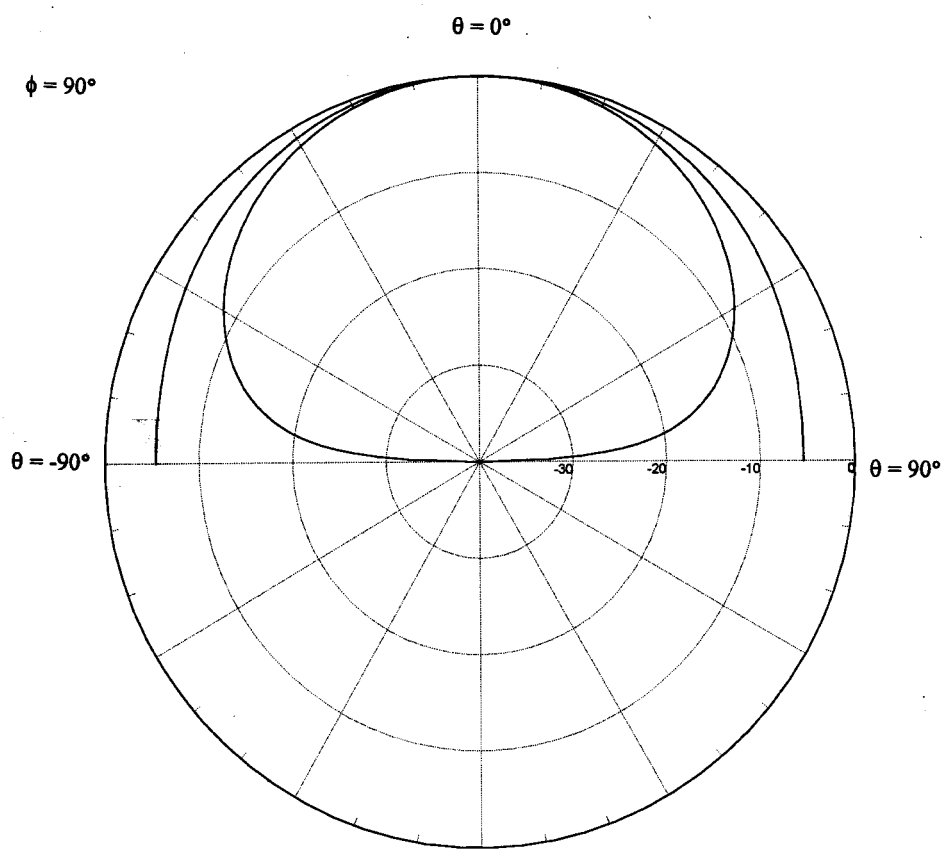

Figure 6.10. The far-field radiation patterns of the rectangular patch antenna in Figure 6.3, modeled using the cavity model in Section 5.2.1.

6.3 Numerical Analysis of the Proximity-Fed Rectangular Patch Microstrip Antenna

6.3.1 The Proximity Coupled Rectangular Patch Microstrip Antenna

The proximity coupled microstrip patch antenna, presented in Section 5.3.4, uses a two layer stacked substrate. The patch is printed on the upper side of the top substrate, and is fed via proximity coupling to a microstrip transmission line printed between the substrate layers. The ground plane is on the lower side of the bottom substrate. The proximity-fed rectangular patch microstrip antenna (MSA) considered in this section is illustrated in Figure 6.11. The feedline is centered with respect to the width of the patch, *W*. The input impedance of the antenna in Figure 6.11 is adjusted by changing the patch width, feedline inset, *S*, and the thickness, d_2, and dielectric constant, ε_r, of the patch substrate.

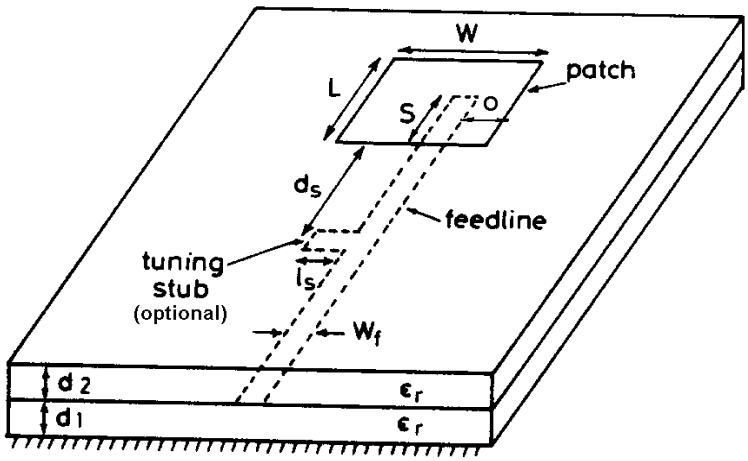

Figure 6.11. The proximity-fed rectangular patch MSA presented in Section 5.3.4. [1]

In the remainder of this section, the effect of antenna geometry on the input impedance of the proximity-fed rectangular patch MSA is modeled numerically using SONNET. The antenna is subsectioned using s = 0.125 cm. The sidewalls spacings are

$a = b = 1.5\lambda$. The top cover location is $c = \lambda$. These dimensions were established using the convergence tests in Section 6.2.3. The proximity coupled rectangular patch antenna in Figure 6.11 is specified in Table 6.2. The dimensions in Table 6.2 are identical to those used in Section 5.3.4. Therefore, comparison with the published results in [1] is useful for verification purposes. The input impedance of the proximity coupled rectangular patch modeled using SONNET is compared to the published result in Figure 6.12.

Table 6.2. Specifications of a proximity-fed rectangular patch MSA

Quantity	Value	Unit
Resonant Frequency	3.5	GHz
d_1	1.58	mm
d_2	1.58	mm
Material (both layers)	Duroid 5880	--
ε_r	2.20	--
l_s	6.5	mm
d_s	33	mm
W_f	5	mm
L	25	mm
W	40	mm
S	12.5	mm

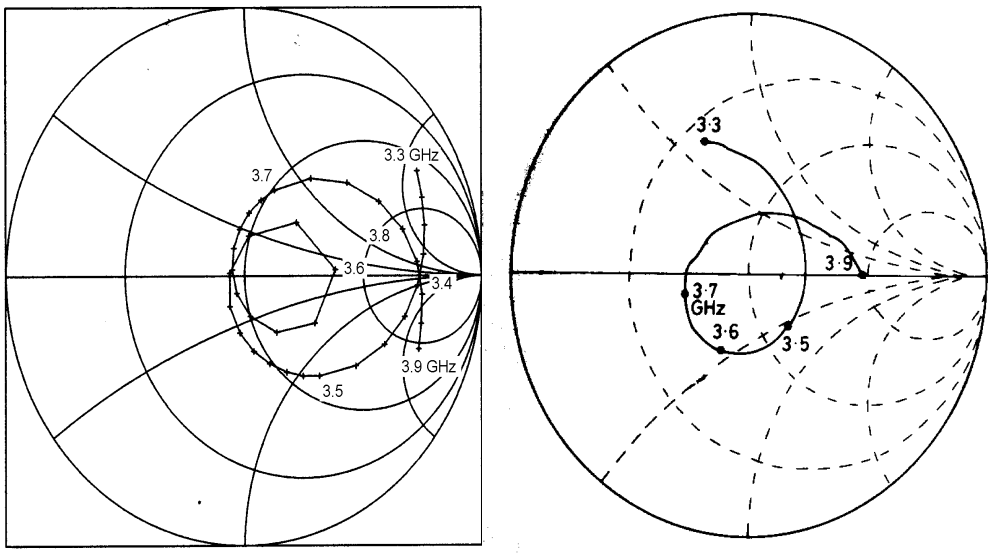

a) b)

Figure 6.12. The input impedance of the proximity coupled rectangular patch in Figure 6.11 and Table 6.2. a) The input impedance neglecting the effect of the optional tuning stub modeled using SONNET. b) The published tuned input impedance including the effect of the tuning stub. [1]

The SONNET data in Figure 6.12(a) does not include the effect of the optional tuning stub in Figure 6.11. The published data in Figure 6.12(b) includes the effect of the stub and is optimized for frequency bandwidth. This accounts for the rotation of the published impedance locus. Other than the rotation, the shape of the impedance locuses correspond well. Both show a double resonance characteristic with the locus centered on the Smith Chart. However, the frequency variation over the published locus is much slower than the modeled variation. Overall, SONNET accurately modeled the behavior of the proximity coupled rectangular patch input impedance.

Figure 6.13 shows that the shape of the proximity coupled rectangular patch antenna radiation patterns are almost identical to those of the probe fed rectangular patch MSA in Figure 6.8. The 3 dB beamwidth in the E-plane is 88° which is 8° narrower than the E-plane beamwidth of the probe-fed rectangular patch MSA. The 3 dB beamwidth in the H-plane is 68°, which is 4° narrower than that of the probe-fed MSA.

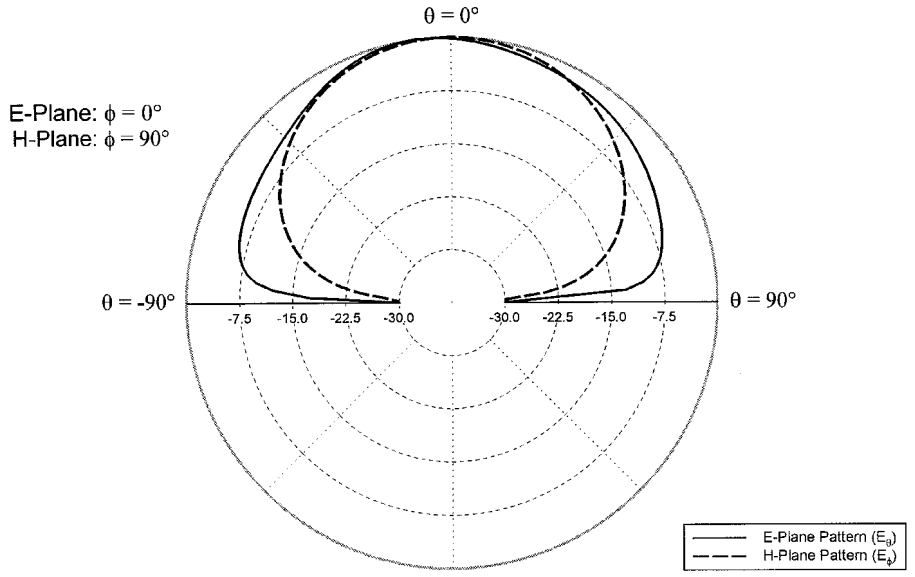

Figure 6.13. The far-field E-Plane and H-Plane radiation pattern of the proximity-fed rectangular patch antenna in Figure 6.11.

In the rest of the chapter, SONNET is used to model the effects of changes in geometry on the input impedance of the proximity-fed rectangular patch MSA. In Section 6.3.2 changes in patch width, *W*, and length, *L*, are made and the input impedances are modeled. In Section 6.3.3 the effects of feedline inset, *S*, and lateral offset, *O*, and antenna substrate thickness, *t*, and dielectric constant, ε_r, on input impedance are presented. Section 6.3.4 involves the effects of a shunt tuning stub on the feedline.

6.3.2 Effects of Patch Size on Impedance

The input impedance of the proximity coupled rectangular patch antenna in Figure 6.11 depends on the width, *W*, and the length, *L*, of the coupled patch. Figure 6.14 shows the input impedance for two different patch widths. In Figure 6.14(a), *W* is increased by 0.5 cm, or 12.5 % of the patch width to *W* = 4.5 cm. In Figure 6.14(b), *W* is decreased by 12.5 % to *W* = 3.5 cm.

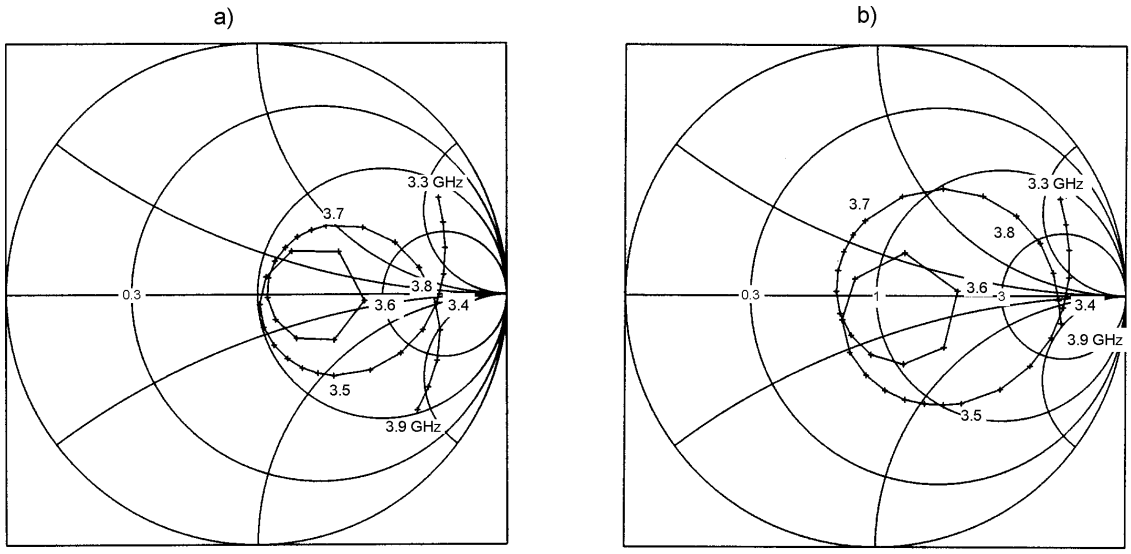

Figure 6.14. The input impedance of the proximity coupled rectangular patch antenna in Figure 6.11 and Table 6.2 when the width of the patch, *W*, is a) increased 12.5 % to *W* = 4.5 cm and b) decreased 12.5 % to *W* = 3.5cm.

Figure 6.14 shows that changing the width of the proximity-fed rectangular patch adjusts the input impedance of the antenna. Figure 6.14(a) shows that increasing the width of the antenna increases the input resistance at most frequencies and decreases the resonant frequencies of the antenna. An increased patch width makes the input impedance more inductive and decreases the width of the impedance locus. The decreased resonant frequencies and increased input inductance indicate that the patch size required to achieve a given resonant frequency is reduced for a wider patch. For a decreased patch width, Figure 6.14(b) shows that the input impedance decreases, the resonant frequencies increase, the input impedance becomes more capacitive, the diameter of the impedance locus increases and thus the frequency bandwidth decreases.

Voltage Standing Wave Ratio (VSWR) is read from the Smith Chart by drawing a circle centered on the chart and through the load impedance point. VSWR is read from the horizontal axis for $r > 1$. The VSWR on the circle is constant, and VSWR < r everywhere within the circle. Thus, the Smith chart can be used to determine impedance bandwidth. For instance, impedance bandwidth is often measured in terms of VSWR < 2.

A VSWR = 2 circle is shown on the Smith Chart in Figure 6.9. The circle has a radius that is the distance from the center of the Smith Chart to $r = 2$ on the horizontal axis. All input impedance points that fall within the circle correspond to VSWR < 2, and constitute the impedance bandwidth of the antenna. An input impedance locus that is optimized for impedance bandwidth is centered on the Smith Chart with as many impedance points as possible falling within the VSWR < 2 circle. Thus, an input impedance locus that is optimized for impedance bandwidth is centered on the Smith Chart, has a small diameter, and a slow frequency variation. Since neither locus in Figure 6.14 is centered on the Smith Chart, some form of tuning is necessary to optimize the impedance bandwidth in either case (see Section 6.3.4).

The input impedance of the antenna changes dramatically when the length, L, of the proximity coupled rectangular patch MSA is adjusted. Figure 6.15(a) shows the input impedance of the proximity-fed rectangular patch antenna when the patch length is increased by 0.125 cm, or 5 % of the original patch length to $L = 2.625$ cm. Figure 6.15(b) shows the input impedance when the length of the patch is decreased by the same amount to $L = 2.475$ cm. Figure 6.15 shows a dramatic difference in input impedance when the length of the patch, L, is changed by 10%. Figure 6.15(a) shows that when the length of the patch is increased the input impedance of the antenna is rotated clockwise around the Smith Chart. This corresponds to an increase in input inductance indicating that the antenna is operating above resonance. When the length of the patch is decreased, Figure 6.15(b) shows that the input capacitance increases indicating that the antenna is operating below resonance. Thus, changing the patch length, L, changes the electrical length of the antenna. The positions of both impedance locuses on the Smith Chart indicate that reactive tuning is necessary to optimize impedance bandwidth and input impedance at resonance. The length of the patch changes the input impedance and resonant frequency of the antenna. Therefore, to achieve a specific resonant frequency, a balance of geometrical parameters and reactive tuning is required to optimize performance.

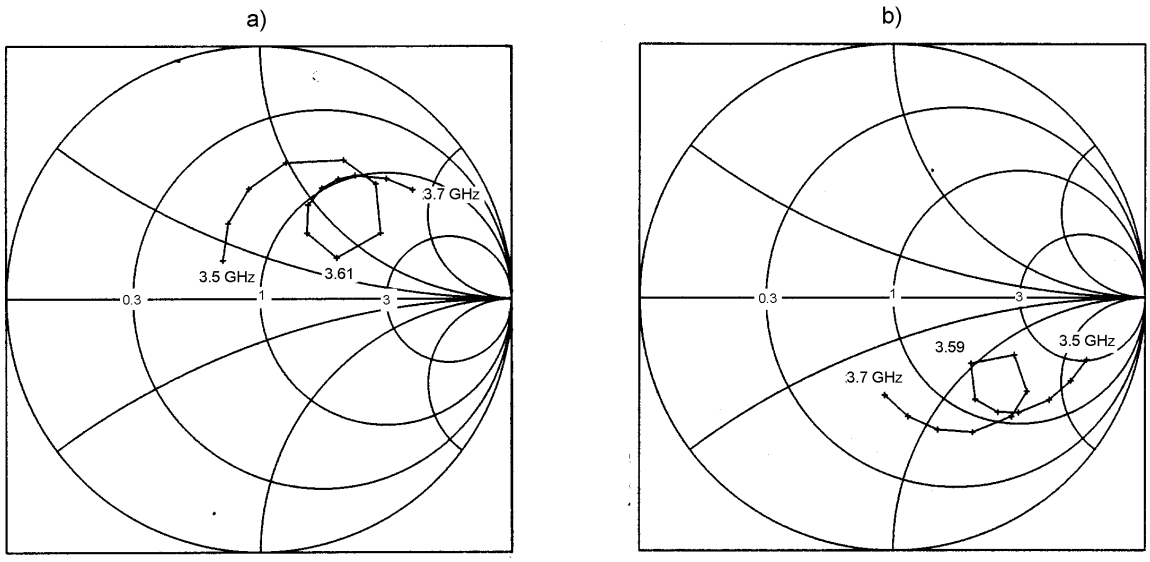

Figure 6.15. The input impedance of the proximity coupled rectangular patch antenna in Figure 6.11 and Table 6.2 when a) the patch length, L, is increased 0.125 cm to L = 2.625 cm and b) the patch length is decreased by 0.125 cm to L = 2.475 cm.

This section treated the effect of patch size on the input impedance of the proximity-fed rectangular patch antenna. In the next section, the effect of feedline placement is presented.

6.3.3 Effects of Feedline Location on Input Impedance

The input impedance of the proximity-fed microstrip patch antenna is adjusted by changes in feedline position. The position of the feedline is described by an inset, S in Figure 6.11, and an offset, O. The inset describes the location of the feedline between the radiating edges of the patch. The offset describes the lateral location of the feedline.

As shown in Figure 6.16, the offset of the feedline does not have a strong effect on the input impedance of the proximity coupled rectangular patch. Figure 6.16(a) shows the input impedance when the feedline is offset 0.5 cm to the left (O = -0.5 cm), and Figure 6.16(b) shows the input impedance for the same offset to the right (O = 0.5 cm).

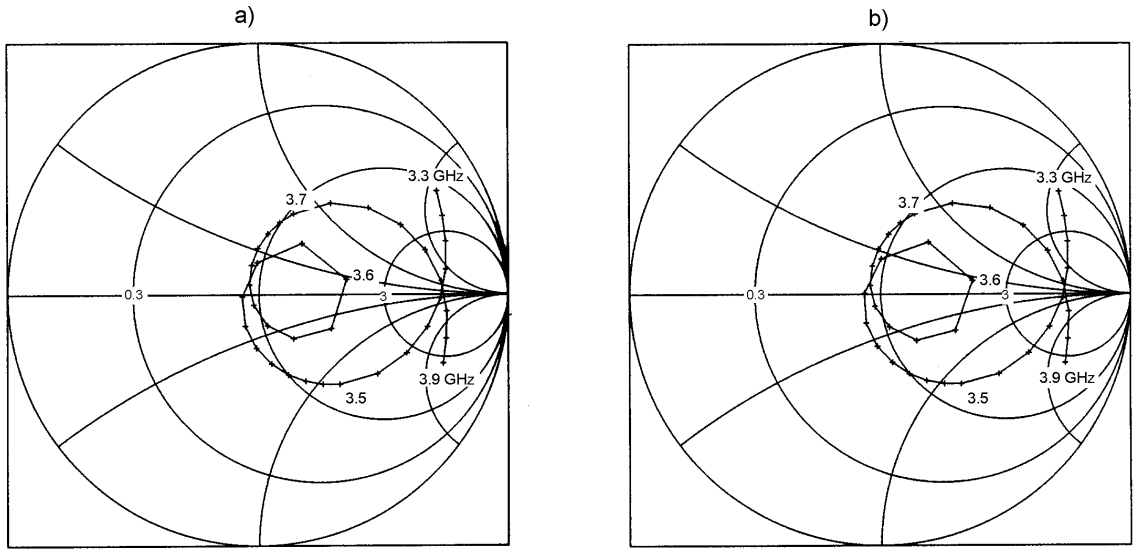

Figure 6.16. The input impedance of the proximity coupled rectangular patch antenna in Figure 6.11 and Table 6.2 when a) O = -0.5 cm and b) O = 0.5 cm

Figure 6.16 shows that feedline offset does not strongly affect the input impedance of the proximity coupled rectangular patch MSA. The differences between Figures 6.16(a&b) and the input impedance for the proximity-fed rectangular patch antenna with no feedline offset in Figure 6.12 are slight. There is no noticeable difference between Figures 6.16(a&b).

Adjusting the feedline inset, S, strongly affects the input impedance of the proximity-fed rectangular patch antenna. Figure 6.17(a) shows the input impedance for an increase in feedline inset of 0.5 cm, S = 0.5 cm, which is 40 % of the original inset, and 20 % of the length of the patch, L. Figure 6.17(b) shows the input impedance for a decrease in inset of the same magnitude, S = -0.5 cm.

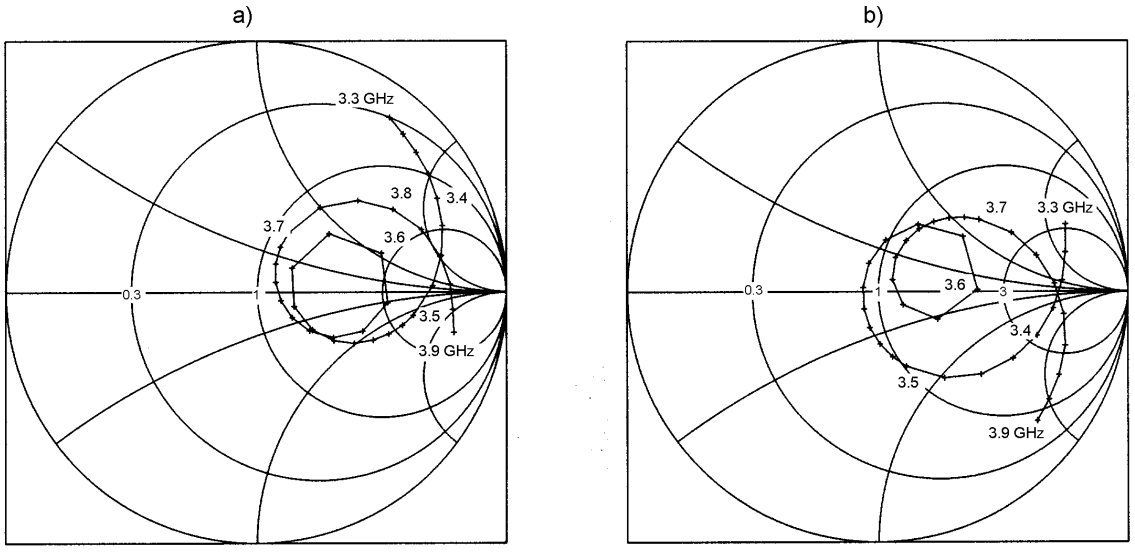

Figure 6.17. The input impedance of the proximity coupled rectangular patch antenna in Figure 6.11 when a) the feedline inset, *S*, is increased 0.5 cm (S = 0.5 cm) and b) the feedline inset is decreased 0.5 cm (S = -0.5 cm).

Figure 6.17 shows that the feedline inset has a strong affect on the input impedance of the proximity coupled rectangular patch antenna. Figure 6.17(a) shows that when the inset is increased, the resonant frequencies and input impedance of the antenna increase. An increased inset causes a counter-clockwise rotation of the impedance locus around the center of the Smith Chart, corresponding to an increased input capacitance. The diameter of the impedance locus increases with increased inset. Thus, the optimized impedance bandwidth is decreased. When the inset is decreased, Figure 6.17(b) shows that the resonant frequencies decrease, the input impedance increases and becomes more inductive, the impedance locus has a decreased diameter and is rotated clockwise around the center of the Smith Chart. Thus, although a decreased inset allows a wider impedance bandwidth and slightly reduced resonant frequencies, it leads to an increased input resistance and reactance and some form of tuning is necessary to optimize bandwidth.

Another factor that tunes the input impedance of the proximity-fed rectangular patch antenna is the thickness of the patch substrate, d_2. Figure 6.18(a) shows the input impedance for a 0.108 cm decrease in d_2 to d_2 = 0.05 cm which is 68 % of the original

substrate thickness. Figure 6.18(b) shows the input impedance when d_2 is increased by 0.142 cm to d_2 = 0.3 cm which is 190 % of the original substrate thickness.

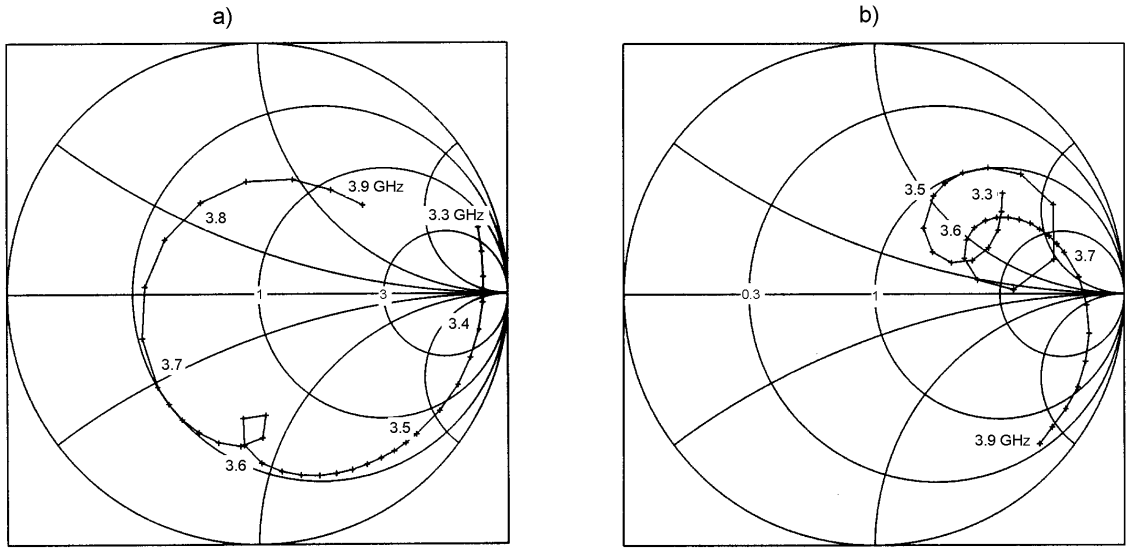

Figure 6.18. The input impedance of the proximity coupled rectangular patch antenna in Figure 6.11 when a) the thickness of the patch substrate is decreased by 68 % to d_2 = 0.05 cm and b) the thickness of the patch substrate is increased by 90 % to d_2 = 0.3 cm

Figure 6.18(a) shows that when the thickness of the patch substrate is decreased, the input capacitance increases. A high VSWR occurs across the band, and the resonant frequencies change dramatically. The input resistance at the first resonance is very high, and at the second is very low. The diameter of the impedance locus becomes very small indicating that, even with reactive tuning, the optimized impedance bandwidth is very small. Figure 6.18(b) shows that when the thickness of the patch substrate is increased, a second loop is introduced into the impedance locus. Thus, with tuning, the optimized impedance bandwidth is dramatically increased. With increased substrate thickness, the input resistance of the antenna is increased and the input reactance becomes more inductive.

The dielectric constant of the patch substrate, ε_r, changes the wavelength of the modes in the dielectric cavity between the conducting patch and the ground plane. An

increased dielectric constant decreases the wavelength in the cavity by a factor that is on the order of

$$x = \sqrt{\varepsilon_r} \ . \tag{6.3}$$

The result is a decrease in the antenna dimensions required for operation at a given resonant frequency. As shown in Figure 6.15, this has a profound effect on the input impedance of the proximity coupled rectangular patch antenna. Figure 6.19(a) shows the input impedance when the dielectric constant is decreased to $\varepsilon_r = 1.8$, or 81% of the original dielectric constant. Figure 6.19(b) shows the input impedance when the dielectric constant is increased to $\varepsilon_r = 4.5$, or 204 % of the original dielectric constant.

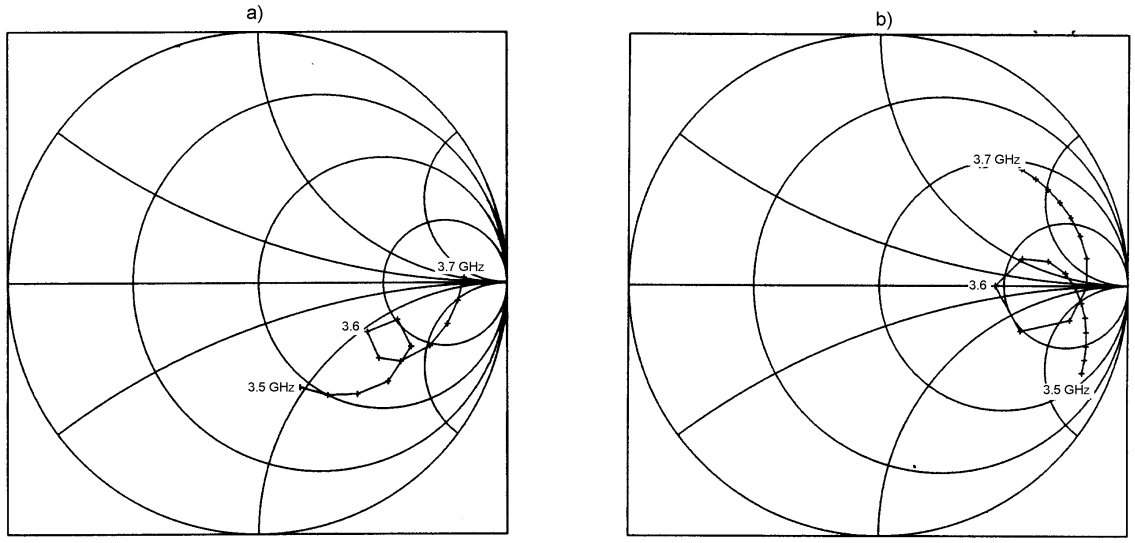

Figure 6.19. The input impedance of the proximity coupled rectangular patch antenna in Figure 6.11 when a) dielectric constant of the substrate is decreased to 1.8 and b) the dielectric constant of the substrate is increased to 4.5.

Figure 6.19(a) shows that when the dielectric constant of the antenna substrate is decreased, the input impedance increases and becomes more capacitive. The same behavior occurs when the patch length is shortened. In Figure 6.19(b), the increased dielectric constant causes the impedance locus to rotate 180°. The resulting input impedance at resonance is much higher than the original case.

Figures 6.14 through 6.19 show that the input impedance and resonant frequencies of the proximity-fed rectangular patch antenna are adjusted by changing the geometry of the antenna. However, reactive tuning is often necessary to optimize the impedance bandwidth of the antenna. In the next section, the impedance bandwidth of the proximity-fed rectangular patch MSA is optimized using reactive tuning.

6.3.4 Effects of Tuning with a Single Open-Circuit Shunt Stub

In the previous section, the input impedance of the proximity coupled rectangular patch antenna was tuned using slight geometrical changes. Most of the changes resulted in input impedance locuses that were not centered on the Smith Chart, and therefore not optimized for impedance bandwidth. In Figure 6.11 a single open-circuited shunt stub of length l_s is located along the transmission line a distance d_s from the edge of the patch. In general, the purpose of the shunt stub is to select d_s so that the admittance, Y, looking into the line at a distance d_s is $Y_o + jB$ where Y_o is the characteristic impedance of the line. The length of the stub, l_s, is adjusted so that the stub reactance is $-jB$ and the result is a matched condition. [4] To limit spurious radiation, the length of the stub is restricted to values much less than $\lambda/2$. If the stub location, d_s, is a multiple of $\lambda/2$, standing waves on the section of feedline between the stub and the patch cause radiation. [1] Thus, it is desirable to tune the antenna with as short a stub as possible placed at a distance from the patch edge that is not a multiple of a half-wavelength.

To tune the proximity coupled rectangular patch MSA, the input impedance is measured or calculated at the edge of the patch. The input impedance, $Z_A = R_A + jX_A$, is measured for the frequency that is to be matched, f_m. The impedance at a distance d_s along the transmission line is [4]

$$Z = Z_0 \frac{(R_A + jX_A) + jZ_0 t}{Z_0 + j(R_A + jX_A)t} \tag{6.4}$$

where Z_0 is the characteristic impedance of the line and $t = \tan(\beta d_s)$. The admittance at d_s is [4]

$$Y = G + jB = 1/Z \tag{6.5}$$

where

$$G = \frac{R_A(1+t^2)}{R_A^2 + (X_A + Z_0 t)^2} \tag{6.6}$$

and

$$B = \frac{R_A^2 t - (Z_0 - X_A t)(X_A + Z_0 t)}{Z_0\left[R_A^2 + (X_A + Z_0 t)^2\right]}. \tag{6.7}$$

To match the antenna to the line, d_s is chosen so that $G = Y_o = 1/Z_o$. Thus [4]

$$Z_0(R_A - Z_0)t^2 - 2X_A Z_0 t + (R_A Z_0 - R_A^2 - X_A^2) = 0 \tag{6.8}$$

is solved for t using the quadratic equation, [4]

$$t = \frac{X_A \pm \sqrt{\frac{R_A\left[(Z_0 - R_A)^2 + X_A^2\right]}{Z_0}}}{R_A - Z_0} \qquad R_A \neq Z_0$$

$$t = \frac{-X_A}{2Z_0} \qquad R_A = Z_0 \tag{6.9a\&b}$$

Solving for t using (6.9a) or (6.9b), the two principal solutions for d_s are [4]

$$\frac{d_s}{\lambda} = \begin{cases} \frac{1}{2\pi}\tan^{-1} t & ,t \geq 0 \\ \frac{1}{2\pi}\left(\pi + \tan^{-1} t\right) & ,t < 0 \end{cases} \tag{6.10}$$

Once d_s is determined, the required length of the stub, l_s, is found by substituting t into (6.7) to find the required stub suseptance, B. This value is used in

$$\frac{l_s}{\lambda} = -\frac{1}{2\pi}\tan^{-1}\left(\frac{B}{Y_0}\right) \tag{6.11}$$

to give the required length of the stub. If the length given by (6.11) is negative, $\lambda/2$ is added until a positive value is achieved. [4]

To demonstrate that a single open-circuit stub tuner can be used to optimize the impedance bandwidth of an arbitrary proximity-fed rectangular patch antenna design, an antenna like that in Figure 6.11 was modeled without a tuning stub, and using the dimensions in Table 6.2. To increase the mismatch, the width of the patch, *W*, was increased to 4.5 cm and the feedline inset, *S*, was decreased to 0.75 cm. The input impedance in Figure 6.20 was calculated at the edge of the patch using SONNET.

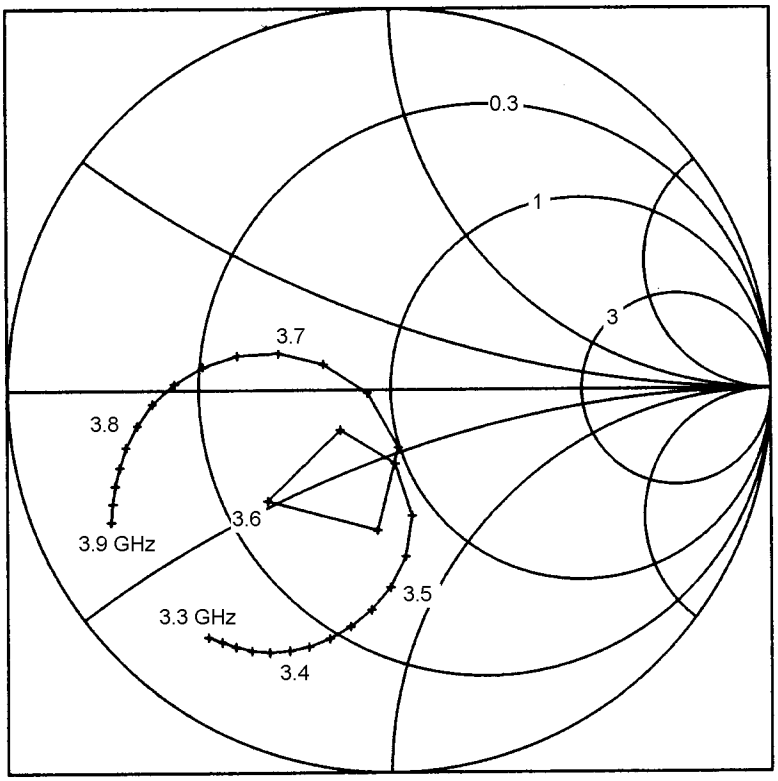

Figure 6.20. The input impedance of the proximity coupled rectangular patch antenna with increased patch width and decreased feedline inset. The reference plane is at the edge of the patch.

In order to optimize the impedance bandwidth of the antenna, the impedance locus in Figure 6.20 should be centered on the Smith Chart. The input impedance in Figure 6.20 is lower and more capacitive than desired. To tune the impedance locus to the center of the Smith Chart, a single open circuit stub tuner is designed using the procedure in (6.4) through (6.11). The impedance is to be tuned to 50 Ω at 3.6 GHz. The input impedance at

3.6 GHz, $Z_A = R_A + jX_A$, is 22.2 - j15.75. Using (6.9a), the solutions for t are -0.2 and 1.336. The corresponding solutions for d_s, from (6.10), are 0.469λ and -0.031λ. Only the positive solution is valid so

$$\underline{d_s = 0.469\lambda = 3.9 \text{ cm.}}$$

Since d_s is nearly 0.5λ, a standing wave will occur on the feedline and cause undesired radiation. Thus, in practice, the width of the patch, W, and feedline inset, S, would be adjusted until a suitable solution for d_s was determined. For this demonstration, however, the undesirable value of d_s is noted and the tuning process continues. To find the length of the stub, l_s, the solution for t (t = -0.2) is substituted into (6.7). The resulting solution for B, B = 0.019, is used in (6.11) to yield

$$\underline{l_s = 0.0379\lambda = 3.2 \text{ cm}}$$

Thus, a single open-circuit shunt tuning stub that is 3.2 cm long is located 3.9 cm away from the patch edge along the feedline. The impedance of the proximity coupled rectangular patch antenna with the addition of the feedline is illustrated in Figure 6.21.

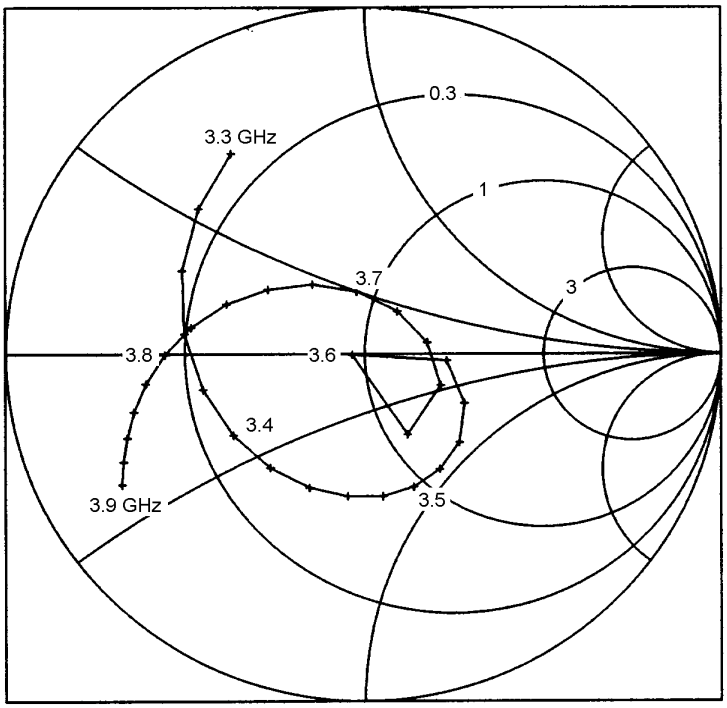

Figure 6.21. The input impedance of the proximity coupled rectangular patch antenna with the addition of the tuning stub.

Figure 6.21 shows that it is possible to tune the input impedance of the proximity-fed rectangular patch antenna to the center of the Smith Chart at any frequency using a single open-circuit shunt stub tuner. Centering the locus on the Smith Chart optimizes the impedance bandwidth. The widest frequency bandwidth is noted on the Smith Chart as a small locus diameter with slow frequency variation around the circumference. If the dimensions of the stub cause undesirable radiation, the geometry of the antenna is changed and the tuning process is iterated. In Figure 6.12(b), the same design process was used by Pozar to center the impedance locus of the proximity coupled rectangular patch antenna on the Smith Chart using a 0.65 cm (0.076λ at 3.5 GHz) stub. The example in Figure 6.12(b) experiences a impedance bandwidth that is 13% of the center frequency.

Thus, it is possible to tune the input impedance of the proximity coupled MSA using changes in antenna geometry and single stub reactive tuning. Optimization for impedance bandwidth at a specific center frequency with a short stub requires an iterative process to balance geometrical with reactive tuning (performed here with a single shunt open-circuit stub). Once tuned, the proximity coupled MSA has a far-field radiation pattern that is similar to that of the MSA using a contacting feed (see Figures 6.13 and 6.10) provided that the stub is short and does not cause spurious radiation. However, the impedance bandwidth of the proximity coupled MSA is much wider, potentially 13% of the center frequency. [1]

6.4 Conclusion

In this chapter, the Method of Moments (MoM) was applied to model the input impedance and far-field radiation of planar antennas. The algorithm was verified by comparing modeled results to results generated using the cavity model presented in Section 5.2.1. The rectangular patch MSA was modeled using both methods and the results showed excellent agreement. The MoM was then used to model the proximity coupled rectangular patch MSA. The results showed that the input impedance of the proximity coupled rectangular patch antenna is strongly tuned by changes in antenna

geometry, material properties, and feedline placement. Combined with reactive tuning, these quantities can be adjusted to optimize impedance bandwidth at a given center frequency. Results in the literature show that the impedance bandwidth of the proximity coupled rectangular patch antenna is potentially 13% of the center frequency. Overall, this numerical study suggests that the proximity coupled rectangular patch MSA is a low profile antenna with a wide impedance bandwidth and radiation characteristics suitable for the hand-held environment.

REFERENCES FOR CHAPTER 6

1. Pozar, D. M., Kaufman, B. "Increasing the Bandwidth of a Microstrip Antenna by Proximity Coupling". *Electronics Letters*, v. 23, Apr. 1987, pp. 368-369

2. Rautio, J. C., Harrington, R. F. "An Electromagnetic Time-Harmonic Analysis of Shielded Microstrip Circuits". *IEEE Transactions on Microwave Theory and Techniques*, v. MTT-35, n. 8, Aug. 1987, pp. 726-730

3. *Sonnet User's Manual*, Volume 1, Part 2: "EM User's Manual". Release 4.0, Sonnet Software, Inc., NY, Sept. 1996.

4. Pozar, D. M. *Microwave Engineering*. Addison-Wesley Publishing Company, Mass., 1990, Chapter 6, Section 2.

CHAPTER 7
CONCLUSIONS AND RECOMMENDATIONS

7.1. Conclusions

The purpose of this discussion was to present design issues for size-reduced and low profile antennas in the hand-held environment. The motivation for the study was the Interactive Video Display System (IVDS) project presented in Chapter 1. In Chapter 2, the fundamental limitations on the performance of electrically small antennas were treated. Closed form representations of the fundamental limitations on radiation Q and efficiency were derived using the work of Chu and Wheeler. Design issues for the hand-held environment were also presented in Chapter 2. These included the effects of a size-reduced ground plane, coupling of energy to the plastic device casing, and coupling of energy to the tissue of the user.

The remainder of the discussion focused on two antenna designs that are well suited for use in hand-held radios. Chapter 3 presented design issues for the Inverted-L Antenna (ILA) and its variations including the Inverted-F Antenna (IFA), Planar Inverted-F Antenna (PIFA), and Dual Inverted-F Antenna (DIFA). Chapter 5 was a discussion of the Microstrip Antenna (MSA) and contained techniques to increase the impedance bandwidth and reduce the size of the MSA.

The theories discussed in Chapters 3 and 5 were tested using numerical modeling and empirical measurement in Chapters 4 and 6. In Chapter 4, a DIFA was designed in the ISM 902-928 MHz frequency band for use in the IVDS described in Chapter 1. The

currents, input impedance, and far-field radiation patterns of the DIFA were modeled numerically using the Method of Moments (MoM), and the Numerical Electromagnetics Code version 4 (NEC4). The model calculations were verified using empirical measurement of the input impedance and radiation patterns of the DIFA. The measurements were made using the Virginia Tech Antenna Lab. In Chapter 6, the proximity-coupled rectangular patch MSA was modeled numerically using the Method of Moments and SONNET (a commercially available software package). The input impedance and far-field radiation patterns of the antenna were calculated. SONNET was also used to determine the affect of antenna geometry on the input impedance of the proximity-coupled rectangular patch antenna.

In summary, this discussion has provided a comprehensive treatment of electrically small and low-profile antenna designs for use in hand-held radios. The current theory was summarized for the hand-held environment, and two applicable antenna designs. The DIFA and proximity-coupled rectangular patch MSA were treated in depth as antenna designs well suited for hand-held radios.

7.2. Recommendations

The following future efforts are recommended:

- Modeling and Measurement of the DIFA using planar horizontal elements.
- A detailed study of the DIFA loaded with dielectric material to provide further size-reduction and increased support to the free end of the antenna.
- Empirical treatment of the Proximity-Coupled Rectangular Patch MSA
- A full study of the Sectoral Circular Patch MSA in Section 5.4.2.

VITA

Andrew Gobien was born in Ann Arbor, Michigan and grew up in Springfield, Virginia. He graduated from Robert E. Lee High School in Springfield, Virginia in 1990 and began studying electrical engineering at Virginia Tech in the fall of that year. In 1994 he completed a bachelor's degree with an English minor and began graduate school, joining the Virginia Tech Antenna Group as a Graduate Research Assistant (GRA). There he worked as an antenna engineer on the Interactive Video Display System (IVDS) for the Interactive Return Services (IRS) Company between 1994 and 1997. In the fall of 1997, Andrew will relocate to Boynton Beach, Florida where will participate in the Engineering Rotation Program at Motorola's Paging Products Division.